Weather and Climate Extremes 43 (2024) 100647

Contents lists available at ScienceDirect

Weather and Climate Extremes

journal homepage: www.elsevier.com/locate/wace

The meteorology and impacts of the September 2020 Western United States extreme weather event

Emma N. Russell [a,*], Paul C. Loikith [a], Idowu Ajibade [b], James M. Done [c], Chris Lower [a]

[a] Department of Geography, Portland State University, 1825 SW Broadway, Portland, OR, 97201, USA
[b] Department of Environmental Sciences, Emory University, 400 Dowman Drive, Atlanta, 30322, Georgia
[c] The National Center for Atmospheric Research, 3090 Center Green Dr., Boulder, CO, 80301, USA

ARTICLE INFO

Keywords:
Extreme event
Large-scale atmospheric circulation
Rossby wave breaking
Wildfire weather

ABSTRACT

In September 2020, Western North America was impacted by a highly anomalous meteorological event. Over the Pacific Northwest, strong and dry easterly winds exceeded historically observed values for the time of year and contributed to the rapid spread of several large wildfires. Nine lives were lost and over 5000 homes and businesses were destroyed in Oregon. The smoke from the fires enveloped the region for nearly two weeks after the event. Concurrently, the same weather system brought record-breaking cold, dramatic 24-h temperature falls, and early-season snowfall to parts of the Rocky Mountains. Here we use synoptic analysis and air parcel backward trajectories to build a process-based understanding of this extreme event and to put it in a climatological context. The primary atmospheric driver was the rapid development of a highly amplified 500 hPa tropospheric wave pattern that persisted for several days. A record-breaking ridge of high pressure characterized the western side of the wave pattern with a record-breaking trough of low pressure to the east. A notable anticyclonic Rossby wave breaking event occurred as the wave train amplified. Air parcel backward trajectories show that dry air over the Pacific Northwest, which exacerbated the fire danger, originated in the mid-troposphere and descended through subsidence to the surface. At the same time, dramatic temperature falls were recorded along the east side of the Rocky Mountains, driven by strong transport of high-latitude air near the surface.

1. Introduction

Beginning on 6 September 2020, an exceptional weather event impacted much of the Western United States (US) resulting in widespread impacts. The event led to devastating wildfires spread by extremely strong winds in the Pacific Northwest (Abatzoglou et al., 2021; Mass et al., 2021), an intense air pollution event in Oregon's Willamette Valley (Conrick et al., 2021), and record-setting snowfall in parts of the Rocky Mountains. Impacts across the west lasted several days to weeks, with amplified wildfire activity on 7 and 8 September (Rasmussen et al., 2021), snowfall on 8 to 10 September (National Weather Service [NWS], n.d.-a, n.d.-b), and unhealthy/hazardous air quality from 10 to 17 September (US Environmental Protection Agency [EPA], n.d.). In this paper, we document the evolution of several key meteorological variables leading up to and during the event using synoptic analysis and air parcel back trajectories for locations representing a diverse range of event impacts.

During the weather event, fire impacts were greatest across the state of Oregon where over one million acres burned (Oregon Department of Emergency Management [ODEM], n.d.), largely attributable to the rapid spread of five 'megafires' (larger than 100,000 acres) beginning on 7 September (Rasmussen et al., 2021). 84% of the burned area was within the forests of the western Cascade Mountains (Rasmussen et al., 2021), resulting in what was likely the most severe wildfire season for the western Cascades in at least the last 120 years (Abatzoglou et al., 2021). However, evidence for similar or even larger fires over the region exists in paleo- and dendro-ecological records (Reilly et al., 2022). While most of the acres burned were classified as forest, several more developed communities across Oregon were directly impacted by the two largest wildfires, the Lionshead and Beachie Creek, that cumulatively burned nearly 400,000 acres in the Cascades (ODEM, n.d.), leading to significant structural loss and damage in the Detroit Canyon and elsewhere. Additionally, two wind-driven fires outside of the Cascades were notable: the Almeda Drive Fire which brought an extensive loss of property and life to urban communities in southern Oregon, and the Echo Mountain Fire which devastated a community near Lincoln City,

* Corresponding author.
E-mail address: emrus2@pdx.edu (E.N. Russell).

https://doi.org/10.1016/j.wace.2024.100647
Received 7 June 2023; Received in revised form 17 January 2024; Accepted 29 January 2024
Available online 30 January 2024

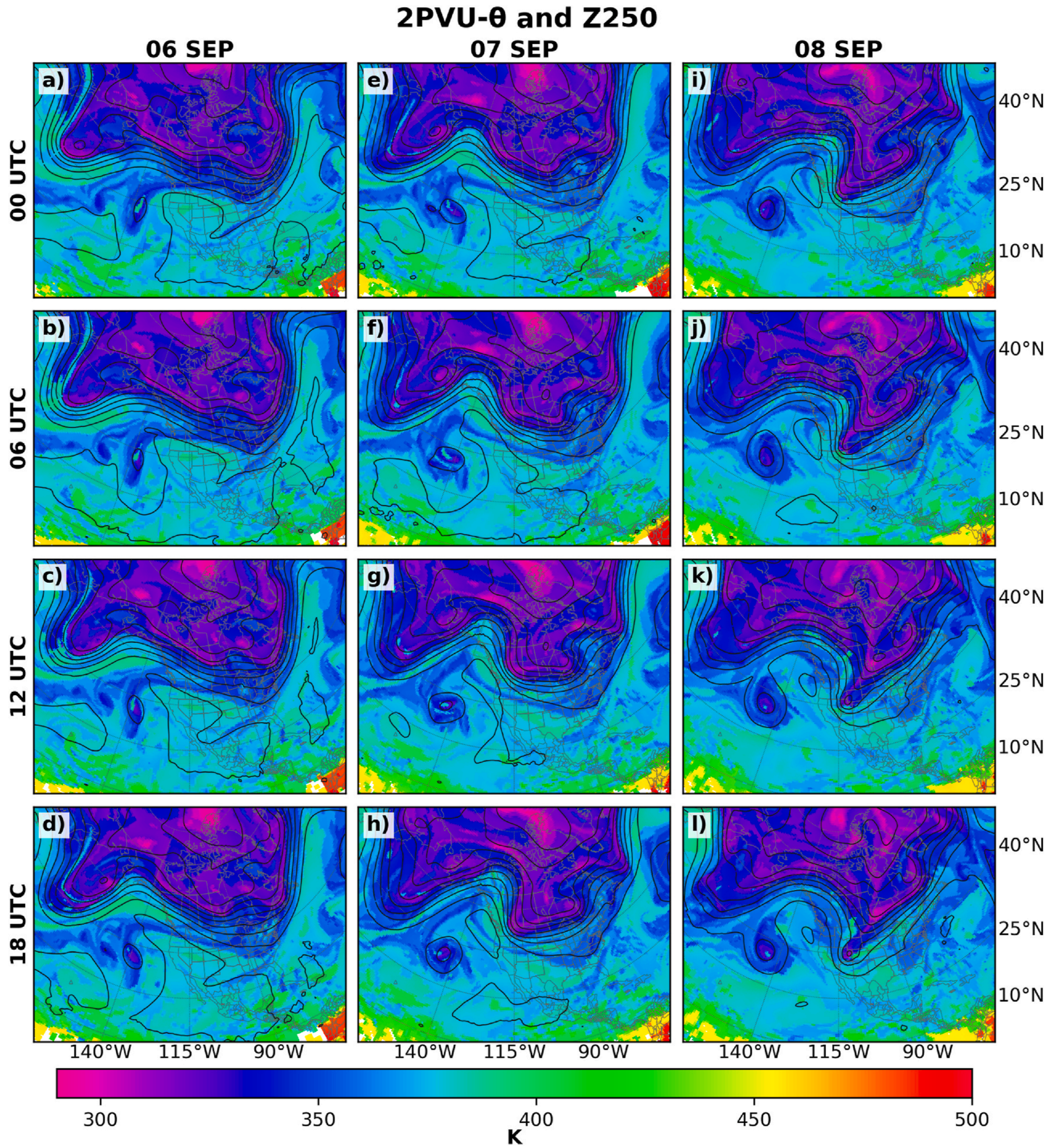

Fig. 1. Potential temperature on the 2 PVU surface (in K, shaded) and 250 hPa geopotential height (contoured every 120 m) over North America at 00, 06, 12, and 18 UTC on (a–d) 6 September, (e–h) 7 September, and (i–l) 8 September.

Oregon. While most of the wildfire activity was confined to Oregon, the Babb fire also largely destroyed the eastern Washington city of Malden (Mass et al., 2021).

This wildfire activity across Oregon prompted local non-profits, volunteer groups, and religious organizations to provide food and temporary shelter for thousands of displaced individuals (Braverman et al., 2021; Oregon Department of Transportation [ODOT], 2022). This rapid migration was further complicated by a range of hazardous conditions including rock falls, landslides, downed trees and powerlines, and the significant destruction of several state highways (ODOT, 2022). The wildfires across Oregon ultimately led to the evacuation of over 40,000 people, destruction of 5000 homes and businesses, and loss of nine lives in the state (ODOT, 2022). The event has also been estimated to be the most economically impactful disaster in Oregon, with a current recovery cost of $355 million and an estimated $5.9 billion in economic impacts on Oregon's Forestry Sector (ODOT, 2022; Rasmussen et al., 2021).

Shortly after the rapid spread of fires in the Oregon Cascades, widespread wildfire smoke led to abnormally high levels of air pollution across the region. The fires, combined with easterly winds, resulted in the transportation of smoke into the Willamette Valley (Conrick et al., 2021). As a consequence, large portions of the state experienced widespread smoke for nearly two weeks, specifically from 7 to 18 September. The Portland, Oregon Metro area experienced eight days of very unhealthy/hazardous $PM_{2.5}$ concentrations from 10 to 17 September, including five consecutive days of hazardous levels ($\geq$250.5 μg/m^3), which became the most extreme $PM_{2.5}$ pollution event in at least the last 24 years (EPA, n.d.). Additionally, Portland and several other cities across the state (Eugene, Bend, Medford, and Klamath Falls) reached record-high Air Quality Index (AQI) levels on either 12 or 13 September (Oregon Department of Environmental Quality, 2020). The smoke led to widespread air pollution exposure as it blanketed much of Oregon and portions of Washington and California and continued to spread across the US in the following days (Juliano et al., 2022).

Oregon's healthcare facilities experienced a 24.9% increase

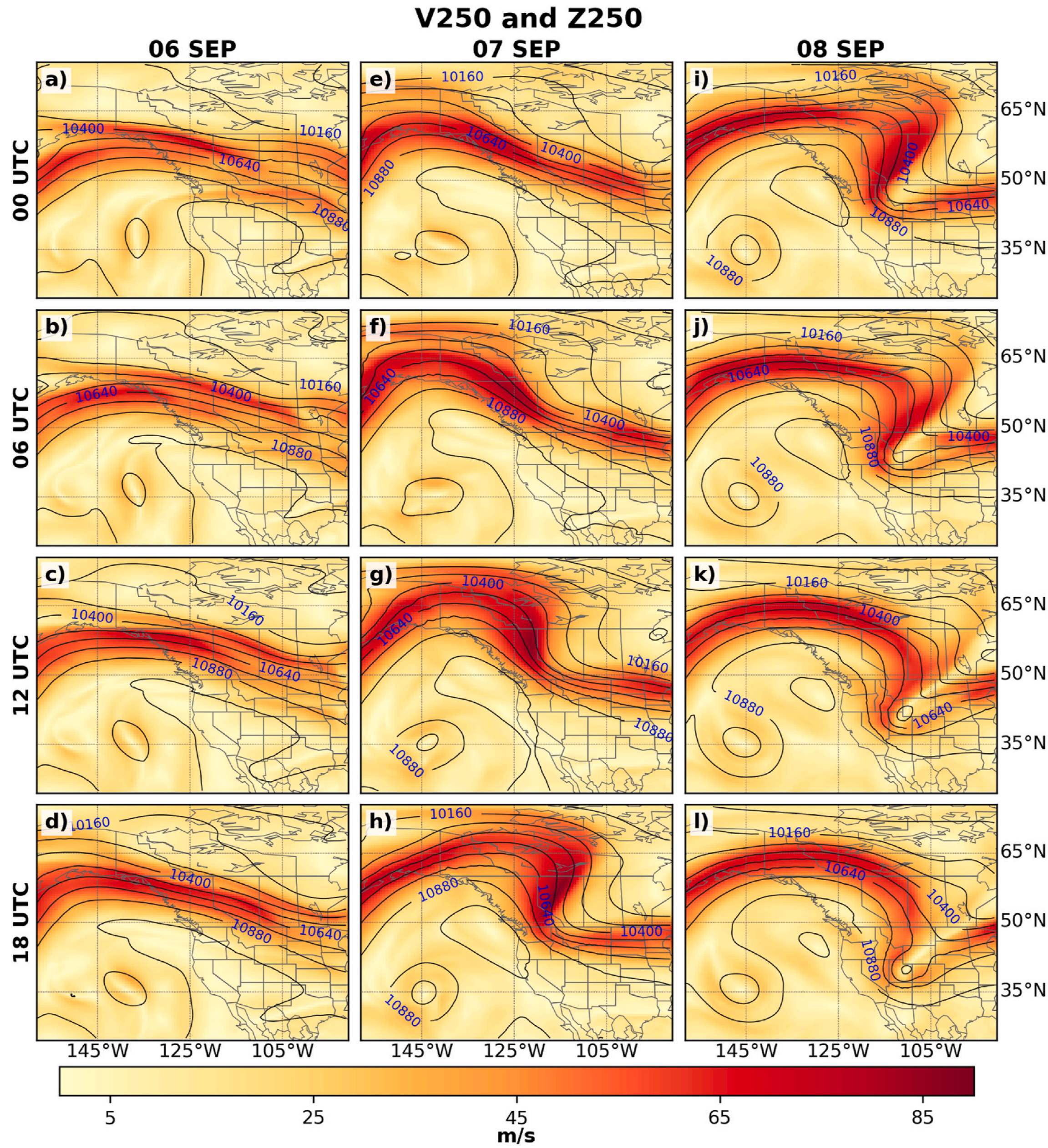

Fig. 2. 250 hPa wind speed (in m/s, shaded) and 250 hPa geopotential height (contoured every 120 m) over Western North America at 00, 06, 12, and 18 UTC on (a–d) 6 September, (e–h) 7 September, and (i–l) 8 September.

statewide in urgent care and emergency department admissions due to smoke-induced respiratory distress (Trenga, 2023). Hispanic and Latino populations were disproportionately impacted with these groups seeking care for asthma-like symptoms at a rate 6.6% higher than the state average (Trenga, 2023). Additionally, persistent headaches, sleeping difficulties, anxiety, and depression were frequently noted health issues wrought by prolonged exposure to wildfire smoke (Braverman et al., 2021). The smoke also created challenges for individuals experiencing breathing difficulties due to COVID-19 by further compromising their lung health (US Centers for Disease Control and Prevention, 2023), and the enhanced $PM_{2.5}$ concentrations may have led to more COVID-19 deaths during this pollution event (Zhou et al., 2021).

In addition to the wildfires and air pollution in the Pacific Northwest, the same weather system brought record-setting cold temperatures for the time of year to parts of the Rocky Mountains, the US Southwest, and the US Great Plains, just days after record-setting warmth. For example, Denver, Colorado recorded its warmest temperature (33.9 °C on 7 September) ever for a day preceding measurable snow (25 mm on 8 September; NWS, n.d.-a). Winter-like conditions followed summer-like weather in other cities including Grand Junction, Colorado, which set a daily precipitation and daily low temperature record on 8 September (NWS, n.d.-b).

The meteorology associated with the wildfire impacts in the US Pacific Northwest has been documented by Abatzoglou et al. (2021) and Mass et al. (2021). They demonstrated that exceptionally strong and dry downslope easterly winds on 7 and 8 September facilitated the rapid spread of several fires, particularly in the Oregon Cascades, compounded by dry conditions and low fuel moisture. Such downslope wind events are common drivers of rapid and destructive wildfire spread under dry conditions in the Western US (Abatzoglou et al., 2023; Mass and Ovens, 2019; Nauslar et al., 2018), and easterly winds are associated with wildfire conditions in the Pacific Northwest (Gedalof et al., 2005). At the synoptic scale, a highly amplified blocking pattern in the mid-to-upper troposphere developed, a pattern previously associated

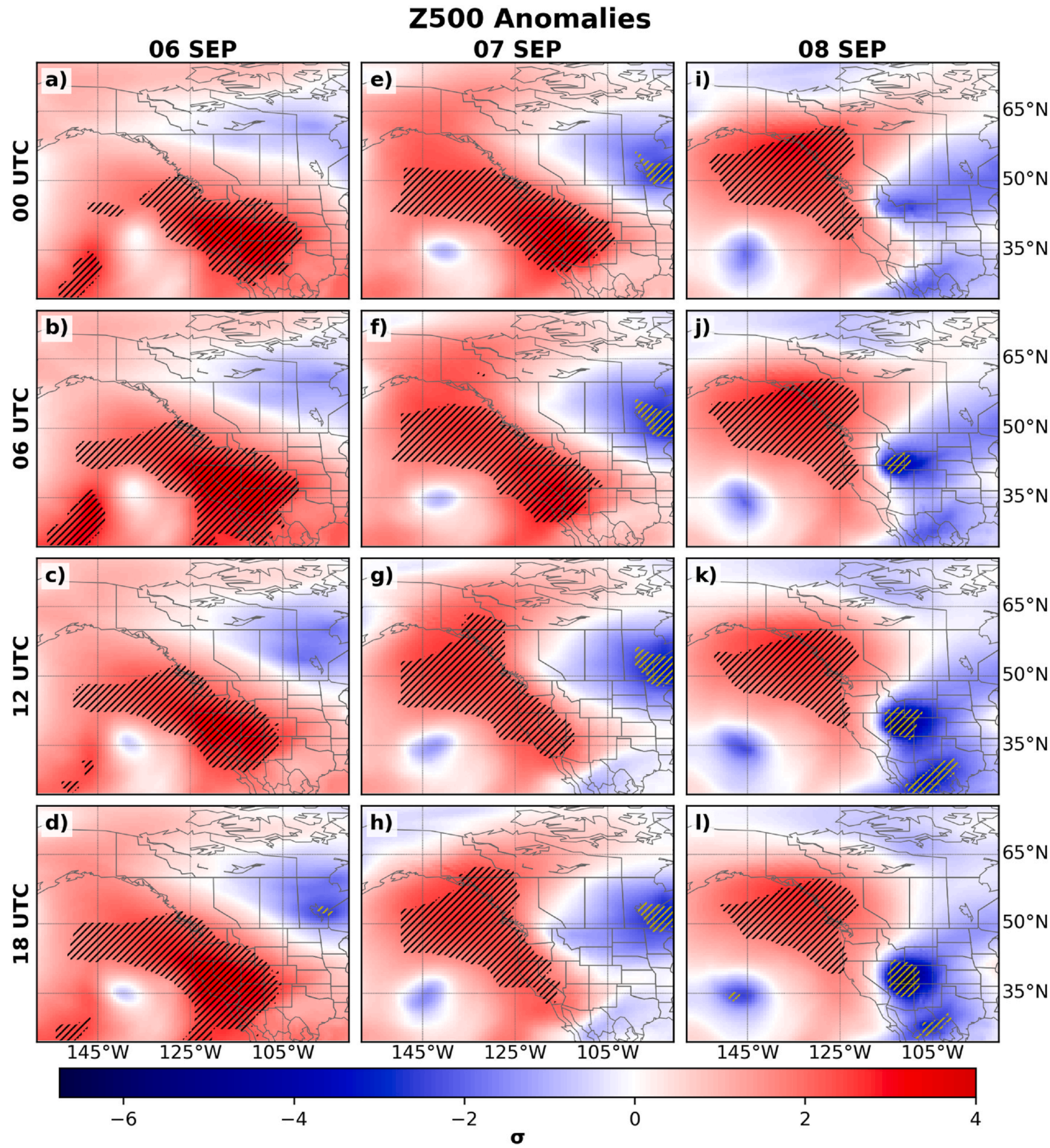

Fig. 3. 500 hPa geopotential height anomalies (in standard deviations, shaded) over Western North America at 00, 06, 12, and 18 UTC on (a–d) 6 September, (e–h) 7 September, and (i–l) 8 September. Standard deviations are computed by dividing Z500 values at each time step by the standard deviation of the calendar day's Z500 frequency distribution. Grid cells with record high (low) geopotential height relative to the daily mean Z500 climatology for the calendar day are marked with black (gray) hatching.

with wildfires in the Pacific Northwest (Gedalof et al., 2005; Hostetler et al., 2018; Jain and Flannigan, 2021; Sharma et al., 2022; Trouet et al., 2009). Here we build on Abatzoglou et al. (2021) and Mass et al. (2021) by expanding analysis beyond the Pacific Northwest and using air parcel back trajectories to diagnose the dynamics and thermodynamics that made this event so historic.

2. Data and methods

All gridded atmospheric data are from the Modern-Era Retrospective Analysis for Research and Applications, Version 2 (MERRA-2), provided on a 0.5° latitude by 0.625° longitude grid (Gelaro et al., 2017). 500 and 250 hPa geopotential height (Z500 and Z250, respectively), 250 hPa winds, sea level pressure (SLP), and air temperature on pressure levels are provided at a 3-h temporal resolution, while the dynamic tropopause pressure, 2-m dew point temperature (DP2M), and 2-m air temperature data are provided at a 1-h resolution. Potential temperature (θ) was interpolated to the dynamic tropopause, defined as the PVU = 2 surface (1 PVU = 10^{-6} m^2 s^{-1} K kg^{-1}), from the nearest pressure levels. Z500 daily climatological averages, maximums, and minimums were calculated for the historical period of 1980–2019.

Air parcel trajectories for 6 locations across the Western US were computed using the National Oceanic and Atmospheric Administration's Hybrid Single-Particle Lagrangian Integrated Trajectory (HYSPLIT) model, which utilizes a hybrid Lagrangian and Eulerian approach to calculate atmospheric parcel trajectories and dispersion (Stein et al., 2015). The HYSPLIT model was run through the Real-time Environmental Applications and Display sYstem (READY) web-based interface using Global Forecasting System (GFS) archived forecast meteorological data available as a 0.25° latitude-longitude grid (Rolph et al., 2017). We

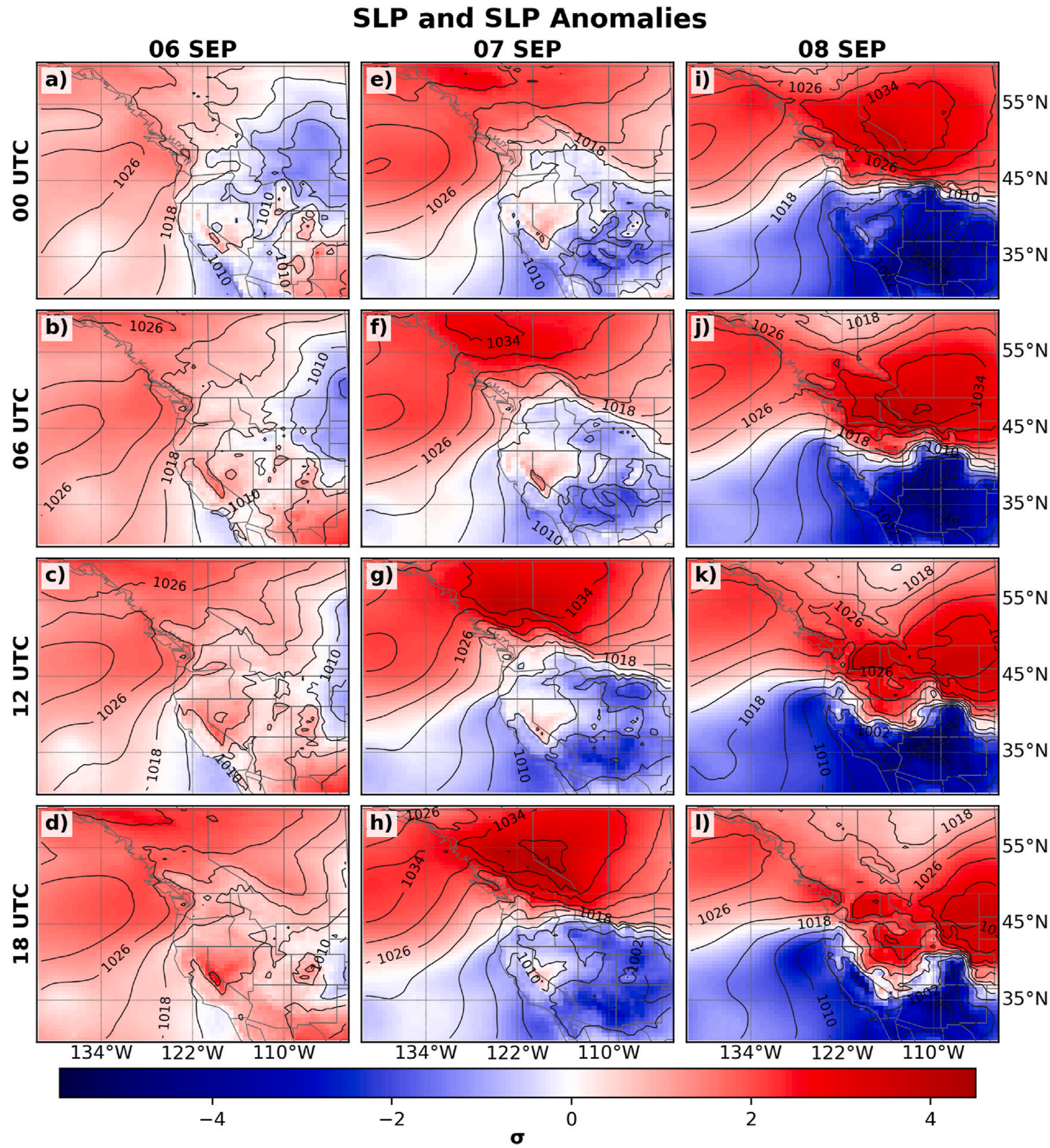

Fig. 4. Sea level pressure (contoured every 4 hPa) and sea level pressure anomalies (in standard deviations, shaded) over Western North America at 00, 06, 12, and 18 UTC on (a–d) 6 September, (e–h) 7 September, and (i–l) 8 September.

note that while we use MERRA-2 as our primary dataset, it is not an available meteorological input in the READY system and was therefore substituted with GFS for parcel trajectories.

3. Results

3.1. Synoptic analysis

One of the key meteorological features of this event was a notable Rossby wave break (RWB) that occurred over Western North America. For this reason, we define the meteorological event of focus as the period leading up to, including, and briefly succeeding the RWB, which was associated with much of the widespread surface impacts including wildfires in the Pacific Northwest and heavy early-season snow in the Rocky Mountain region. Therefore, this study will analyze the meteorological development from 6 to 8 September 2020.

Toward building a synoptic storyline for the event, Figs. 1–6 show the progression of key meteorological fields every 6 h starting at 00 UTC on 6 September and ending at 18 UTC on 8 September. Figs. 1 and 2 depict the upper-level circulation evolution showing potential temperature on the dynamic tropopause (2PVU-θ), Z250, and 250 hPa winds. At 00 UTC on 6 September, a prominent upper-level ridge over the entire Western US is evident by the north-south 2PVU-θ and associated Z250 gradients north of the region (Fig. 1a and 2a). As 6 September progressed, the ridge shifted west and built poleward, resulting in high 2PVU-θ south of Alaska and equatorward extensions of low 2PVU-θ on either side (Fig. 1b-d). This synoptic pattern rapidly changed on 7 September as the ridge south of Alaska expanded northward and the trough to its east surged south with a prominent anticyclonic RWB occurring between 12 UTC and 18 UTC on 7 September over the Northwestern US and Western Canada (Fig. 1e-h). This is also evident in the polar jet in Fig. 2g with a reversal of the westerlies within the jet corresponding to the wave break.

By 00 UTC on 8 September, a prominent upper-level omega block

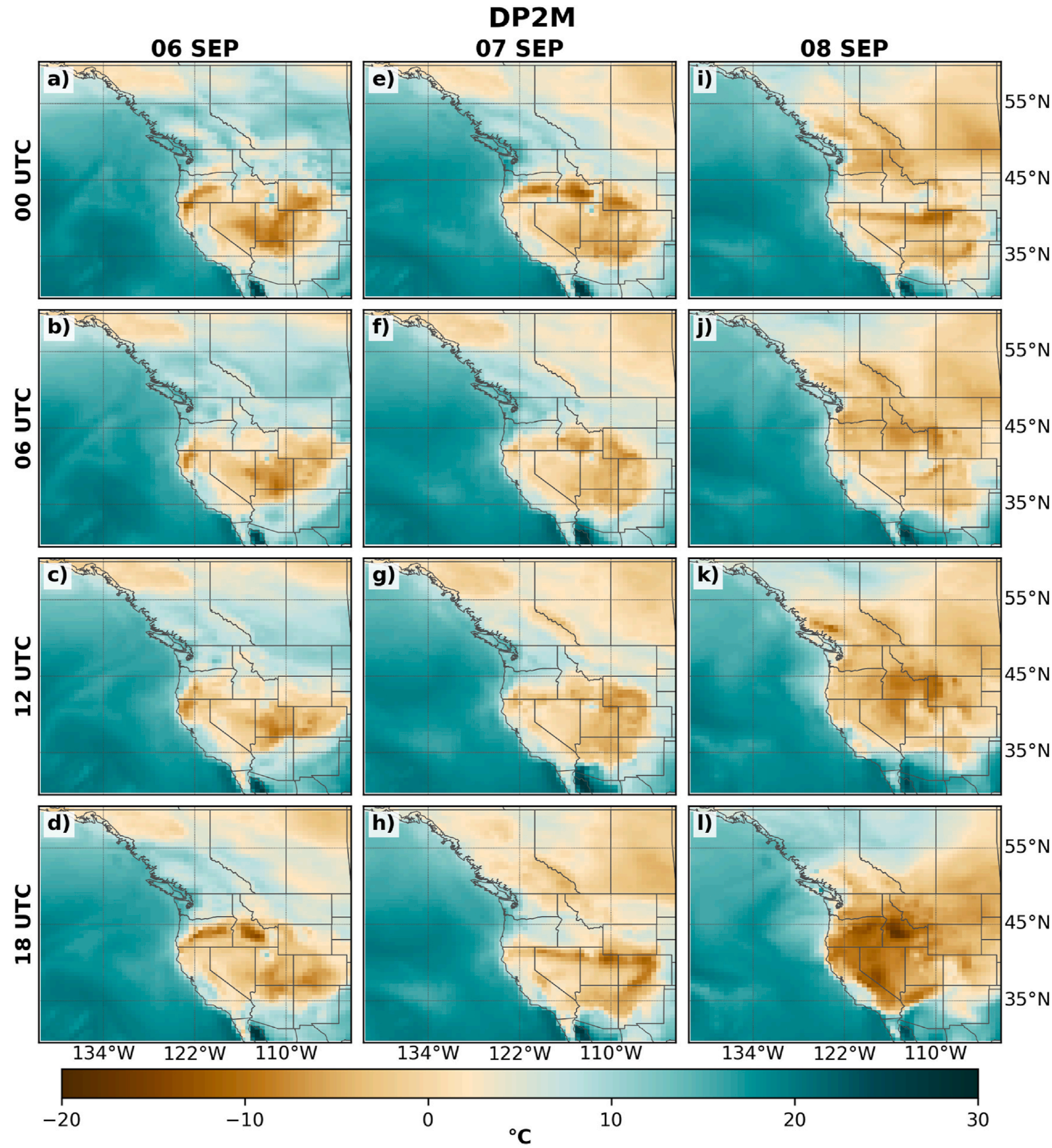

Fig. 5. 2-m dew point temperature (in degrees Celsius, shaded) over Western North America at 00, 06, 12, and 18 UTC on (a–d) 6 September, (e–h) 7 September, and (i–l) 8 September.

centered just west of the Pacific Coast is evident on both the 2 PVU surface (Fig. 1i) and 250 hPa geopotential height and wind fields (Fig. 2i). A region of very low 2PVU-θ for the latitude was drawn into the Southwestern US and a corresponding closed Z250 low developed (Fig. 2k). This upper-tropospheric progression highlights the dramatic amplification of the upper-level dynamics and development of a strong blocking pattern during 7 and 8 September, driving rapid surface weather changes and severe weather impacts across the affected region.

In the mid-troposphere, Z500 anomalies indicate an exceptionally strong and broad ridge (as indicated by daily record Z500 values) present across much of the western conterminous US at 00 UTC on 6 September, with the largest geopotential height anomalies centered over the states of Utah, Arizona, and Nevada (Fig. 3a). The anomalous ridge gradually strengthened and expanded over the northeast Pacific while a weak cutoff low that developed near the 140°W meridian and 35°N parallel slowly strengthened and drifted west (Fig. 3b-d). Z500 was the highest in the MERRA-2 daily climatology record (dating back to 1980) over much of the Western US on 6 September, as seen by the black hatching in Fig. 3, with anomalies exceeding three standard deviations in much of the ridge (Fig. 3a-d).

Major changes to the mid-level synoptic pattern began on 7 September as a rapidly developing trough lowered Z500 first across the northern tier of the US and then over much of the Western US within hours, coincident with the anticyclonic RWB (Fig. 3e-h). At the same time, the Z500 ridge over the northeast Pacific amplified poleward and the cutoff low over the Pacific drifted slowly westward. This created a notable zonally oriented Z500 gradient over the Northwestern US and Western Canada, indicative of a sharp tropospheric airmass boundary. The offshore cutoff low located equatorward of the Z500 ridge created a Rex block-like pattern towards the end of 7 September (Fig. 3h). The strong ridge continued to break record high Z500 for the date while the developing trough on the eastern periphery of the study domain began to break record low Z500 (Fig. 3e-h).

On 8 September, the developing trough continued to propagate

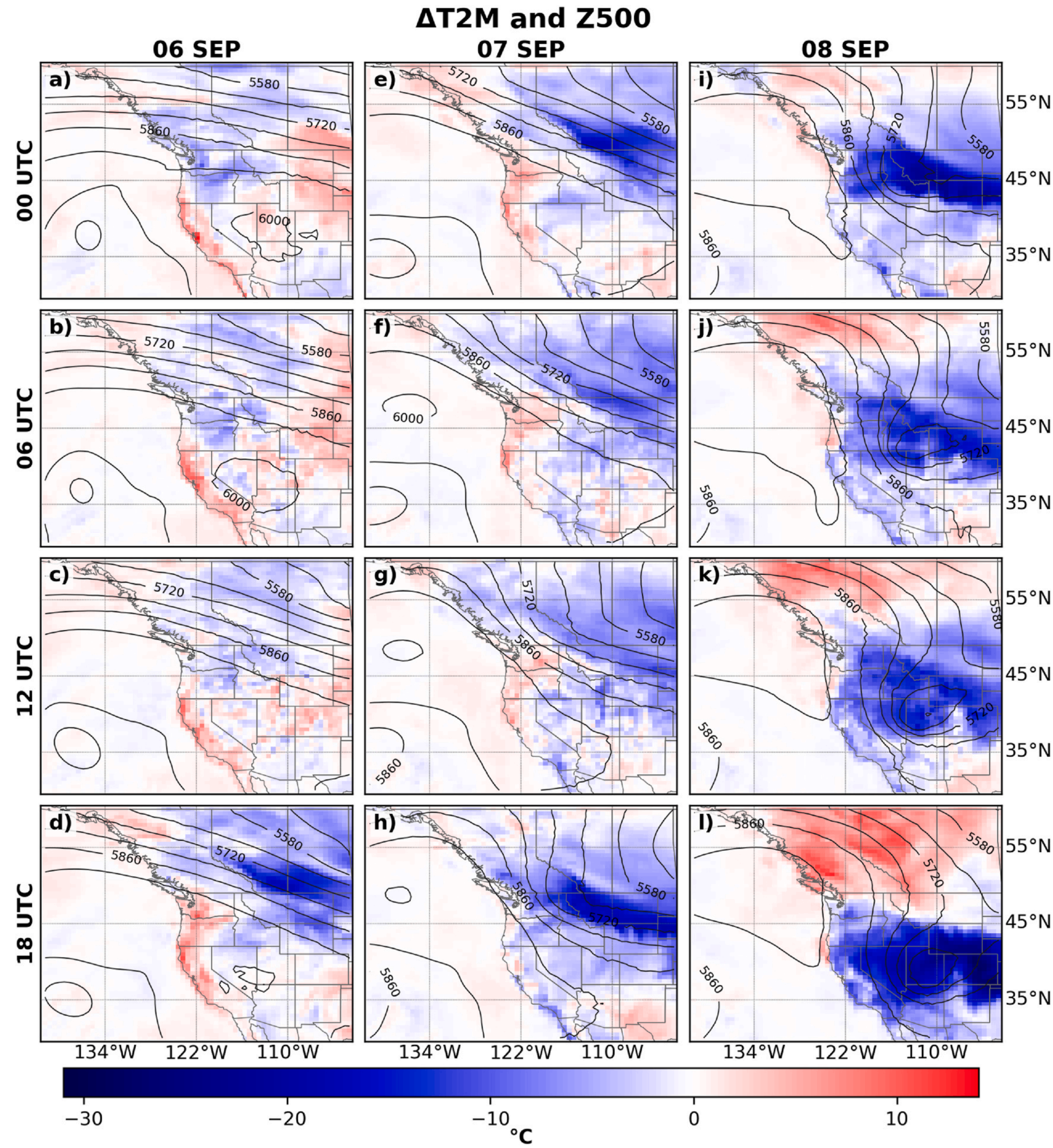

Fig. 6. 24-hour change in 2-m temperature (in degrees Celsius, shaded) and 500 hPa geopotential height (contoured every 70 m) over Western North America at 00, 06, 12, and 18 UTC on (a–d) 6 September (e–h) 7 September, and (i–l) 8 September.

towards the southwest with an area of maximum negative height anomalies and record low Z500, seen by the gray hatching in Fig. 3, centered over Utah at 06 UTC (Fig. 3j). Note that the region of record low Z500 at this time was collocated with the region of minimum 2PVU-θ (Fig. 1j and 3j). The upper-level trough continued to strengthen and resulted in widespread record low Z500 for the date across the Southwestern US, with anomalies over six standard deviations below normal (Fig. 3k and l). Remarkably, many of the grid cells with record low Z500 had record high Z500 only one to two days prior, indicating a highly amplified upper-level pattern over the Southwestern US. It is also notable that by 18 UTC on 8 September, Z500 values in the cutoff low west of the ridge also ranked as the lowest in the MERRA-2 record for the day (Fig. 3l), further evidence of an exceptionally amplified wave pattern. The offshore ridge also continued to break records for maximum Z500 throughout 8 September. Similar to the progression seen on the 250 hPa surface (Fig. 2), a strong 500 hPa Ω block became prominent, stabilizing the highly amplified wave pattern in both time and space during the event (Fig. 3l).

One of the most impactful components of this event was the strong surface winds across the Pacific Northwest that facilitated explosive wildfire growth in the states of Washington and Oregon (Abatzoglou et al., 2021; Mass et al., 2021). The progression of the SLP field and anomalies throughout the event is shown in Fig. 4 to aid in the diagnosis of the drivers of the strong surface winds. On 6 September, a surface high present in the northeast Pacific, offshore of the state of Washington, strengthened (Fig. 4a-d). Lower SLP was present over land to the east and south of the developing high, creating a modest SLP gradient that promoted largely northerly to northwesterly flow across the Pacific Northwest (not shown, can be inferred from SLP gradient).

On 7 September, a strong high pressure began to build and travel southward from northern Canada (Fig. 4e), coincident with the eastern (favoring upper-level convergence) side of the 250 hPa ridge (Fig. 2e). As the record-breaking ridge and trough amplified (Fig. 3e-h), the upper-level convergence over Western Canada and upper-level divergence over

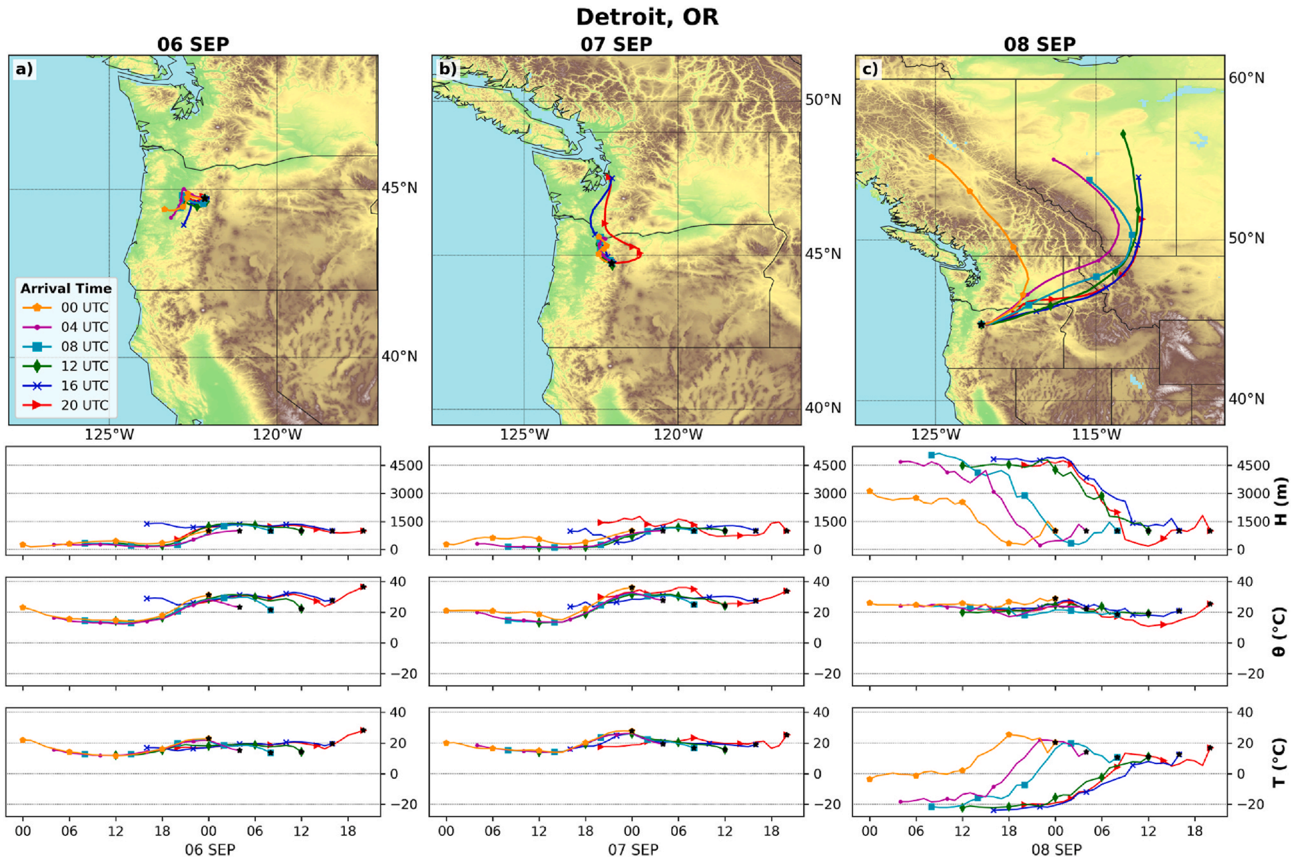

Fig. 7. HYSPLIT 24-h air parcel backward trajectories for Detroit, Oregon on (a) 6 September, (b) 7 September, and (c) 8 September. Trajectory paths are shown on the upper map, while parcel height (H, in meters above mean sea level), potential temperature (θ, in degrees Celsius), and ambient temperature (T, in degrees Celsius) are also plotted along the path. Trajectories are colored and marked based on the hour of arrival at the destination, which is consistent for all dates in the figure.

Colorado resulted in the continued strengthening of the high-and-low pressure system at the surface, respectively. As a result, a very strong pressure gradient developed across the northern tier of the US between these systems (Fig. 4h).

The SLP gradient reached peak strength on 8 September with a very strong gradient between a highly anomalous northern high pressure and southern low pressure (Fig. 4i-l). A thermally induced surface trough was also evident across Western Oregon and Washington at 00 UTC on 8 September, extending from Northern California to the west of Seattle, Washington (Fig. 4i). As SLP continued to increase east of the thermal trough, a surface pressure gradient developed across the Pacific Northwest that was highly conducive to strong offshore surface winds, especially over the Oregon Cascades, the region most impacted by wind-driven fires during this event.

Another main contributor to the wildfire-conducive environment in the Pacific Northwest was the dry conditions that developed over the three-day event (Abatzoglou et al., 2021; Mass et al., 2021). The progression of DP2M across the US is shown in Fig. 5 as an indicator of atmospheric moisture content. On 6 September, the DP2M pattern primarily reflected surface elevation, with higher elevations showing lower DP2M than lower elevations (Fig. 5a-d). Broad decreases in DP2M then occurred across most of the Western US, concurrent with the strong easterly winds in the Pacific Northwest on 7 and 8 September. At 00 UTC on 8 September, DP2M began to decrease rapidly over the Pacific Northwest, first over Western Washington and then over Western and Central Oregon (Fig. 5i). By 18 UTC, very low dewpoints, in many cases well below 0 °C, extended throughout the entire Western US and to the Pacific Coast (Fig. 5l). This rapid decrease in dewpoint followed the RWB event and coincided with the strong offshore winds that drove the extensive and rapidly moving wildfires in Washington and Oregon. The very low dewpoint values that enveloped the region, however, were not advected from a region of lower values, as there was no source region of very low DP2M available for transport. This indicates that the very dry air arrived through a different process which we further explore in Section 3.2.

The effect of the rapid change in synoptic circulation over the three-day event is visualized in Fig. 6 with 24-h change in 2-m temperature (ΔT2M) alongside Z500. While ΔT2M was relatively modest across Western North America on 6 September, large decreases in temperature began to occur on 7 September as the Z500 pattern began to amplify, with a band of negative ΔT2M extending from central Washington and Oregon to the Dakotas by 18 UTC (Fig. 6h). Throughout 8 September, large negative ΔT2M was recorded across much of the Southwestern US with the area of maximum 24-h change progressively migrating to the south and southwest along with the upper-level trough. ΔT2M decreases approaching or exceeding 20 °C occurred across much of the US Southwest with even larger temperature decreases over the southern Great Plains on 8 September (Fig. 6l). This rapid cooling over the Southwestern US resulted in widespread record-breaking cold and precipitation, most notably in the Rocky Mountains.

3.2. *Air parcel backward trajectory analysis*

To better understand the processes driving the highly anomalous surface weather and airmass transport throughout the event, we computed air parcel backward trajectories using the HYSPLIT trajectory model for six affected locations across the Western US. The first four locations analyzed were those impacted by wildfire activity in the Pacific Northwest and include cities across Oregon and Washington. Two additional locations in Colorado that experienced an early-season storm

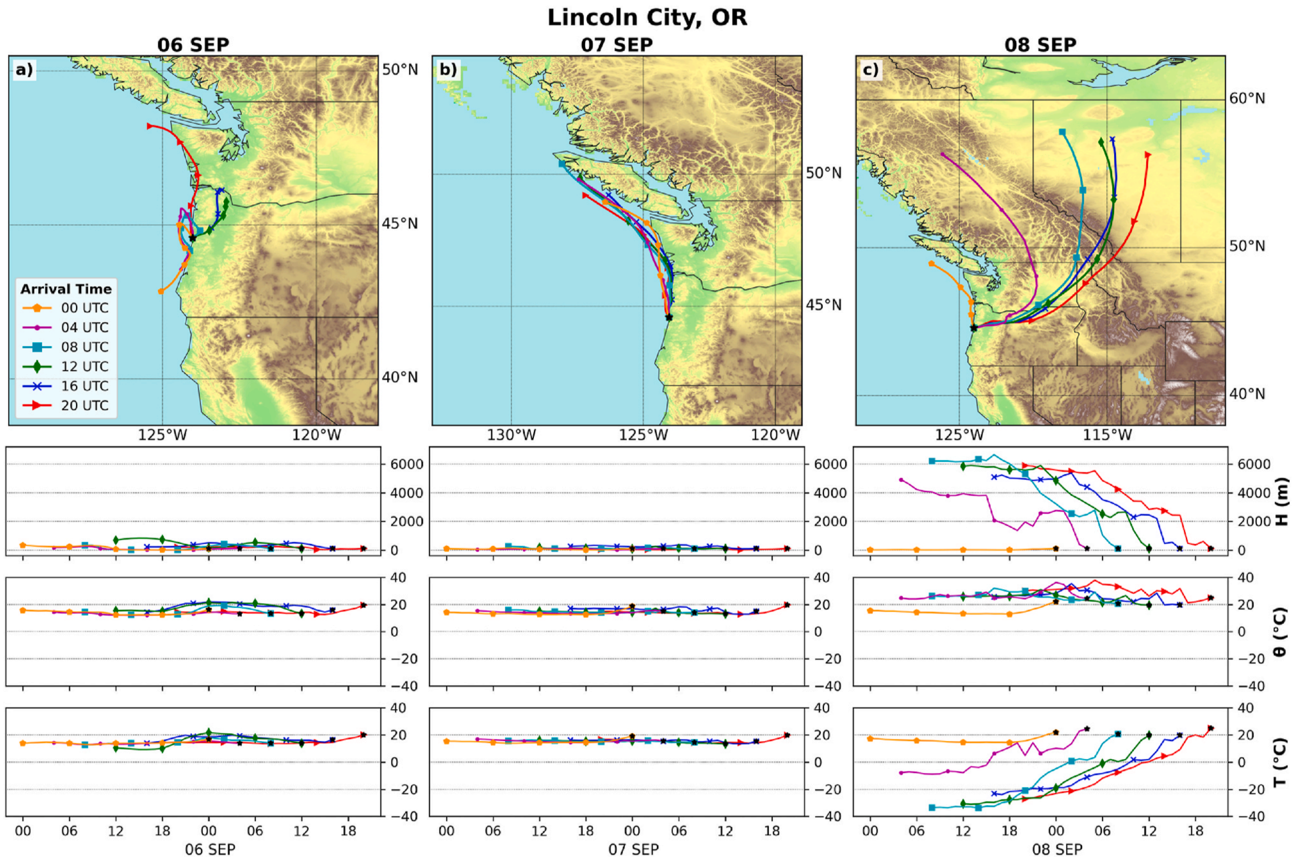

Fig. 8. As in Fig. 7 but for Lincoln City, Oregon.

and cold outbreak were also investigated. Results for Detroit, Oregon, which was severely impacted by the two largest wildfires in the state during this event, the Beachie Creek and Lionshead fires (ODEM, n.d.), are shown in Fig. 7. For each location, air parcel backward trajectory paths were computed for the 24 h before parcel arrival at the location's surface (0 m above ground level) at 4-hourly intervals from 00 UTC on 6 September to 20 UTC on 8 September. For example, the parcel labeled 00 UTC for 6 September arrived at the surface in Detroit at 00 UTC on the 6th with the backward trajectory ending at 00 UTC on 5 September. In addition to parcel location, parcel height (H), potential temperature (θ), and ambient temperature (T) were computed along the trajectory path (bottom panels of Fig. 7).

On 6 September, air parcels arriving in Detroit traveled relatively short distances during the preceding 24 h (Fig. 7a). The parcels remained near the surface and arrived in Detroit from the west, traveling up the Detroit Canyon. Modest diabatic temperature changes reflect the diurnal cycle and very high temperatures for the location were recorded during the daytime hours (Fig. 7a). A similar set of trajectory paths are seen in the first half of 7 September, with localized parcels experiencing little heating throughout their path to Detroit (Fig. 7b).

Parcel origins shifted slightly as 7 September progressed, with parcels arriving in Detroit at 16 and 20 UTC traveling from the Puget Sound region, continuing to originate near the surface and contributing to the anomalously hot weather in Detroit (Fig. 7b, surface high temperatures near Detroit were about 28 °C compared with an average of 23.4 °C). Between 20 UTC on 7 September and 00 UTC on 8 September, a major shift in parcel trajectory occurred with the first parcel on 8 September originating over central British Columbia at 3000 m above mean sea level (Fig. 7c). The descent of the parcel resulted in considerable adiabatic warming. All subsequent parcels traveled from central Alberta and originated near or above 4500 m with their descent resulting in substantial adiabatic warming (and drying, not shown in figure). In combination with the strong winds, indicated by the large distance traveled by the parcels over 24 h, and the hot and dry weather preceding the wind shift, the parcel trajectories help explain the rapid fire spread throughout the event. Additionally, the parcels' origin at 4500 m on 8 September explains the rapid drop in DP2M seen in Fig. 6, as these parcels originated in the dry mid-troposphere hours before arrival at the surface.

A similar series of events is seen in the backward trajectories for Lincoln City, Oregon, a coastal location affected by the Echo Mountain fire (Fig. 8). On 6 September, air parcels originated just off the Pacific Coast and traveled along the coast at the surface to Lincoln City (Fig. 8a). During 7 September, surface-level parcels continued to travel southward, along the coast from the North Pacific Coast with minimal temperature changes along the way (Fig. 8b).

Comparable to what was observed in the Detroit trajectories in Fig. 7, parcel trajectories for Lincoln City drastically changed between 00 UTC and 04 UTC on 8 September, with trajectories shifting from a marine origin to an interior and high-altitude origin over Western Canada within 4 h (Fig. 8c). The first parcel on 8 September originated over British Columbia at around 5000 m above mean sea level, while the remaining parcels arrived from nearly 6000 m above mean sea level over Alberta (Fig. 8c). This anomalously cold air (in an absolute sense), with ambient temperatures nearly −40 °C, experienced strong adiabatic warming during its descent to Lincoln City, with temperatures of some parcels increasing nearly 60 °C during their 24-h descent (Fig. 8c). This warm, dry, and strong offshore wind created critical fire conditions along the typically cool and humid coastline.

The Alameda Drive fire, which caused widespread destruction to the Rogue Valley communities of Phoenix, Talent, and Medford, Oregon was spread by strong easterly winds. Backward trajectories for Medford are shown in Fig. 9, which share commonalities with Detroit and Lincoln City, although the shift in trajectory characteristics occurred a few hours

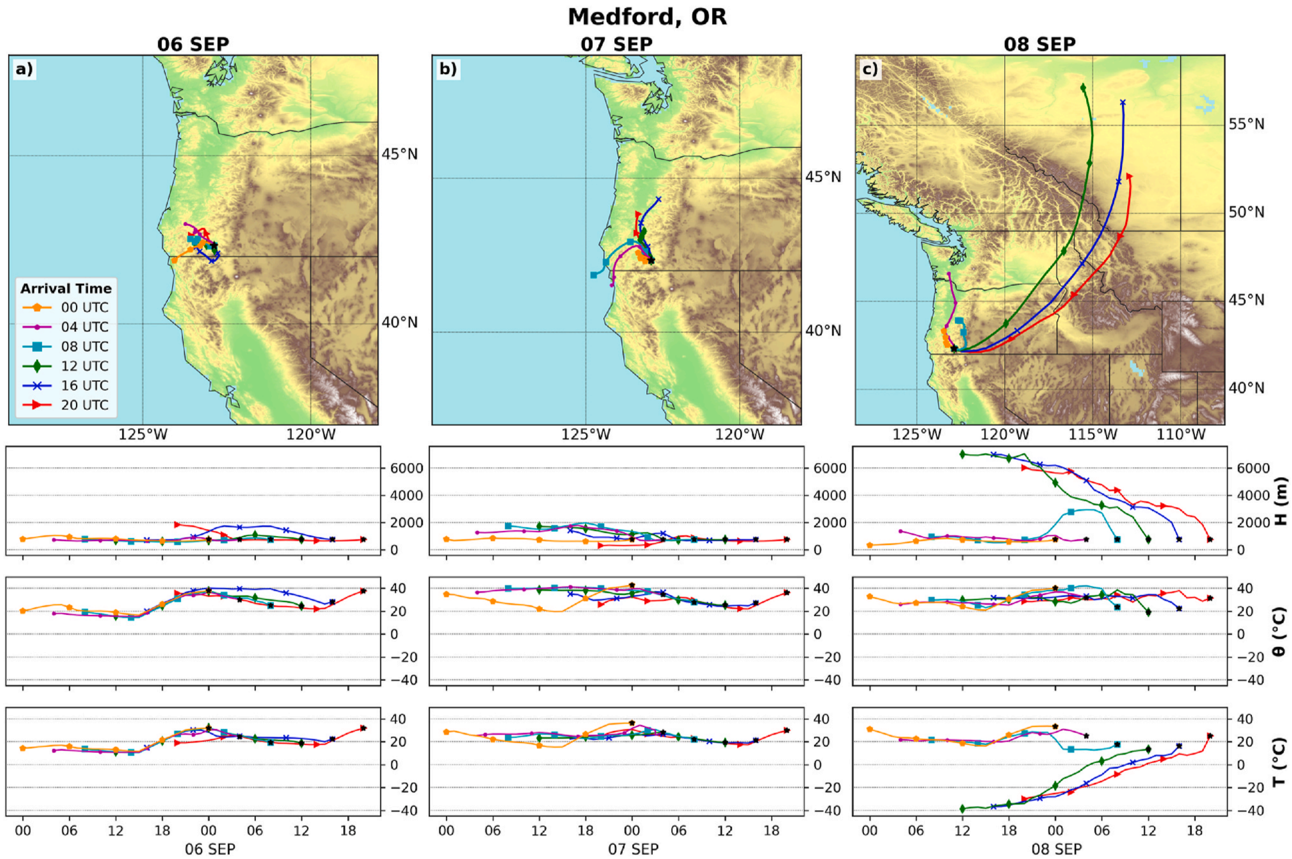

Fig. 9. As in Fig. 7 but for Medford, Oregon.

later than in the previous examples. Trajectories traveling short distances over 24 h, indicating light winds, on 6 and 7 September (Fig. 9a and b) were replaced by parcels originating from Western Canada well over 6000 m above mean sea level on 8 September (Fig. 9c). These parcels underwent strong adiabatic warming and had very low moisture content for surface air in the region, contributing to the critical fire weather in Medford and surrounding areas.

While the fire weather aspects of this event were most notable for the explosive forest fires on the west side of the Oregon Cascades, Eastern Washington, specifically the community of Malden, also experienced severe damage from the Babb Road fire. This fire occurred in a much drier ecosystem, primarily burning grassy vegetation (Mass et al., 2021). Unlike the trajectories in Oregon, winds were relatively strong on the first day of the event in Malden, with parcels traveling from the northern Willamette Valley of Oregon on 6 September (Fig. 10a). A dramatic shift in the parcel trajectories is again present, although this occurred hours earlier than the Oregon trajectories, with the most notable shift occurring at 12 UTC on 7 September when parcels began originating from the northwest at higher altitudes than before (Fig. 10b).

The trajectory paths continued to shift and by the end of 7 September, originated over central Alberta 24 h prior to arrival in Malden (Fig. 10b). This continued to be the case throughout 8 September in a pattern much like those in the previous examples (Fig. 10c). Although similar in origin and distance of travel to the Oregon trajectories, these parcels originated at lower heights and thus experienced less adiabatic warming through descent. The adiabatic warming that did occur while descending to Malden, however, further dried the airmass and in combination with strong surface winds, facilitated rapid fire spread.

This strong and dramatic shift in the movement of tropospheric air across the Pacific Northwest corresponds to the rapid evolution of atmospheric dynamics that occurred during the event. Changes in air parcel origination on 9 September coincide with the anticyclonic RWB event (Fig. 2) and strong development of a mid-tropospheric high over the Pacific Northwest (Fig. 3). The resulting extremely anomalous Z500 ridge resulted in subsidence and the transport of mid-tropospheric air down to the surface in Oregon and Washington. Alongside these upper-level drivers was the development of a strong meridional pressure gradient (Fig. 4), promoting the horizontal advection from higher pressure in Western Canada towards lower pressure in the Western US at lower atmospheric levels. Such Z500 anomaly patterns and HYSPLIT trajectories are also characteristics of other offshore wind-driven wildfire events in the Pacific Northwest (Garner and Kovacik, 2023).

The following trajectories aim to further examine the processes associated with the unseasonable wintry precipitation and cold air outbreak in the Rocky Mountains, with an evaluation of Grand Junction and Denver, Colorado. Both of these regions experienced record-breaking 24-h temperature falls and precipitation as a result of the event. On 6 September, air parcels arriving in Grand Junction traveled relatively short horizontal distances, with parcels arriving in the first half of the day traveling relatively close to the surface (Fig. 11a). By the second half of 6 September, parcels originated at higher altitudes and descended roughly 3000 m, possibly due to convective mixing during the daylight hours (Fig. 11a). On 7 September, parcels began traveling longer distances from the northwest over the 24-h period with the parcels arriving at 16 and 20 UTC showing considerable descent and adiabatic warming (Fig. 11b). However, surface temperatures remained below 30 °C in Grand Junction throughout the day.

As in the Pacific Northwest locations, a dramatic change occurred on 8 September, coinciding with the first day of snow in the region. Parcels traveled from Oregon, Nevada, and Utah during the first half of the day and later shifted to a northeasterly path with parcels coming from Wyoming and Colorado (Fig. 11c). The most notable characteristic of the parcels on 8 September is the diabatic cooling they experienced during

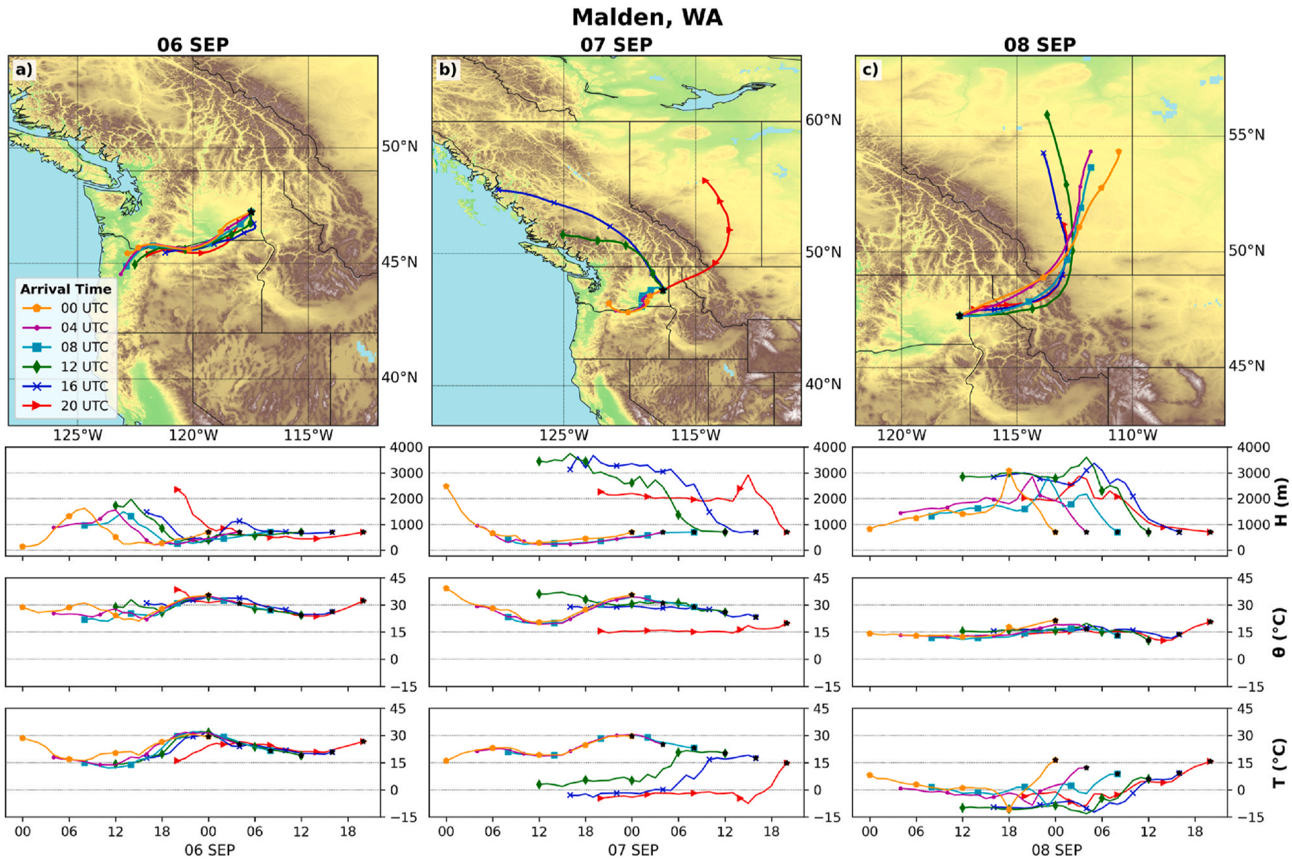

Fig. 10. As in Fig. 7 but for Malden, Washington.

the last portion of their path as they neared Grand Junction, indicated by the synchronous fall in ambient and potential temperatures to near 0 °C (Fig. 11c). This cooling is likely thermodynamically driven from melting and evaporation of hydrometeors rather than advection of cooler air, as initial trajectory parcel temperatures did not cool proportionally compared with the previous two days.

The parcel trajectories show a very different story for Denver compared with Grand Junction. Parcels traveled primarily from the west into Denver on 6 September until a shift toward the north and northeast occurred around the end of the day on 7 September (Fig. 12a and b). This shift coincided with much colder surface temperatures as parcels cooled along the 24-h trajectory. Unlike at Grand Junction, the cooling was adiabatic as parcels ascended the slope of the Great Plains, evident by the potential temperature showing little change along the trajectory paths on 8 September (Fig. 12c). The parcels arriving on 8 September also started colder than the parcels on the previous two days, indicating cold air advection also played a role. While both Colorado locations experienced similar unusual weather, the physical mechanisms for the dramatic cooling and early-season snow were substantially different.

4. Discussion and conclusions

During a multi-day span in the second week of September 2020, an exceptionally impactful synoptic-scale weather event occurred across the western half of North America. Driven by a highly amplified tropospheric wave pattern and ensuing Rossby wave breaking, impacts ranged from historic and destructive wind-driven wildfires across the Pacific Northwest, to record cold and snow over the Rocky Mountains. The anomalously warm conditions present across the region prior to the wave amplification and Rossby wave break resulted in several regions experiencing swings from record or near-record-breaking warmth to record or near-record-breaking cold in a matter of hours, illustrating the dynamic nature of this event. While the direct impacts of the event only lasted two or three days in most locations, lingering hazardous concentrations of smoke from the wildfires spread over much of Western North America and remained under stagnant air conditions for many days (Conrick et al., 2021).

Highly amplified tropospheric blocking events and associated RWB have been associated with severe surface weather across the mid-latitudes including extreme heat and cold (Millin and Furtado, 2022; Pelly and Hoskins, 2003) and enhanced fire weather in the Northwestern US (Zhong et al., 2020). In fact, less than one year after this event, a record-breaking heat wave affected the Pacific Northwest and was also associated with a blocking pattern and record-breaking ridge (Conrick and Mass, 2023; Loikith and Kalashnikov, 2023). While diagnosing the drivers of the wave pattern itself is beyond the scope of this current study, evidence suggests that three western Pacific tropical cyclones that underwent extratropical transition near the Korean Peninsula in the span of 12 days likely contributed to the amplification of the atmospheric wave train responsible for this event (Stuivenvolt-Allen et al., 2021).

Among the many remarkable meteorological and climatological aspects of this event was the timing. Highly amplified wave patterns are uncommon over the region, and the mid-latitudes in general, during the warm season, and become more common as baroclinicity increases later in the fall (Blackmon et al., 1977; Branstator, 1992). While strong easterly winds have historically occurred in early September over the Pacific Northwest and have been associated with the largest fires west of the Cascade Mountains (Reilly et al., 2022), the 950 hPa winds observed in September 2020 were the strongest in the observational record for the time of year in many places (Mass et al., 2021). Had this event occurred later in the fall, after the onset of the Pacific Northwest wet season, the fire impacts would likely have been negligible.

Given the unusual nature of this event, it is reasonable to consider

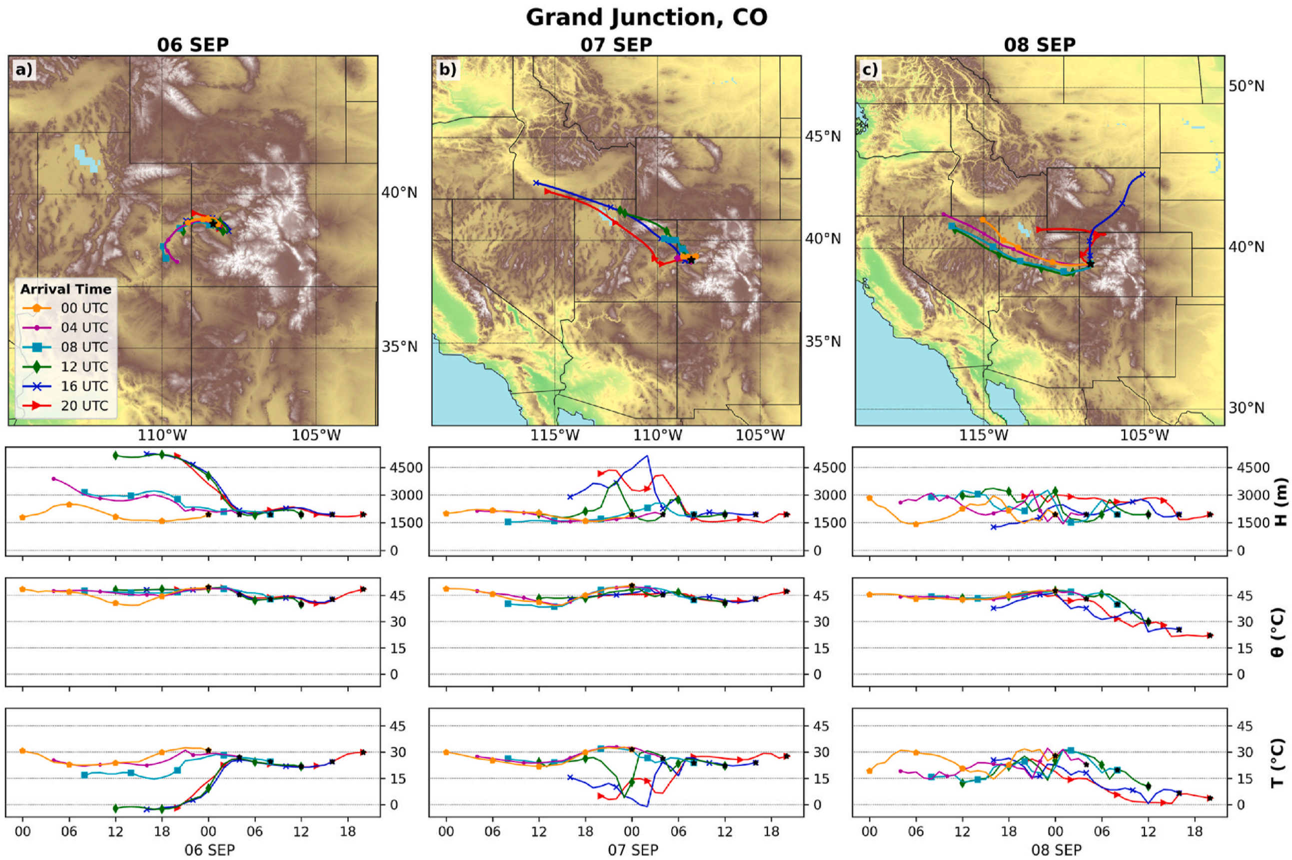

Fig. 11. As in Fig. 7 but for Grand Junction, Colorado.

the ways in which anthropogenic climate change could have played a role in this and future events. While an investigation into the potential roles of global warming for this event is not within the analysis conducted here, we offer some insight. First, it is important to note that attempting to attribute this event to a warming climate is complicated given its many facets, all of which could be influenced by warming differently. Regarding the atmospheric dynamics and associated wind, Hawkins et al. (2022) show that anthropogenic warming has slightly decreased the probability of strong offshore wind events over much of Oregon and California in autumn, although when they occur, they are more likely to coincide with extreme fire conditions due to warmer temperatures. Loikith et al. (2022) show no projected increase in the frequency or strength of ridging under a high-end warming scenario by the end of the 21st century for summer or fall in the region where the ridge was present during this event. Mass et al. (2021) indicate that the energy release component, burning index, and fuel moisture were not unusual for this time of year, but the development of record or near-record-breaking easterly winds led to a rapid reduction in relative humidity and an increase in fire weather indices, suggesting the rare wind event was the primary driver of the wildfire event.

Reilly et al. (2022) also present evidence of similar or larger fires occurring in the region prior to meaningful anthropogenic warming. This all said, mean summer and fall temperature over North America has increased considerably over the past several decades (Vose et al., 2017), which would act to increase the likelihood of hot and dry antecedent conditions in general, but would also decrease the likelihood of the record cold temperatures recorded over the Rocky Mountains. Nevertheless, it is important to learn from and document the drivers of such rare extreme events to facilitate climate change attribution of complex events and as a means of being better prepared for similar future occurrences.

Funding

This work was supported by the National Center for Atmospheric Research [Grant: 245533] (E.N.R., I.A., J.M.D.) and the U.S. National Science Foundation [Grant: AGS-2206997] (P.C.L). This material is also based upon work supported by the Early Career Faculty Innovator Program at the National Center for Atmospheric Research, a program sponsored by the National Science Foundation. Any opinions, findings and conclusions, or recommendations expressed in this material do not necessarily reflect the views of the National Science Foundation. Cooperative Agreement Number: 1755088.

CRediT authorship contribution statement

Emma N. Russell: Data curation, Formal analysis, Methodology, Software, Visualization, Writing – original draft, Writing – review & editing. **Paul C. Loikith:** Conceptualization, Funding acquisition, Methodology, Supervision, Writing – original draft, Writing – review & editing. **Idowu Ajibade:** Funding acquisition, Project administration, Writing – original draft. **James M. Done:** Funding acquisition, Project administration, Writing – original draft. **Chris Lower:** Project administration, Writing – original draft.

Declaration of competing interest

The authors declare that they have no known competing financial interests or personal relationships that could have appeared to influence the work reported in this paper.

Data availability

Data will be made available on request.

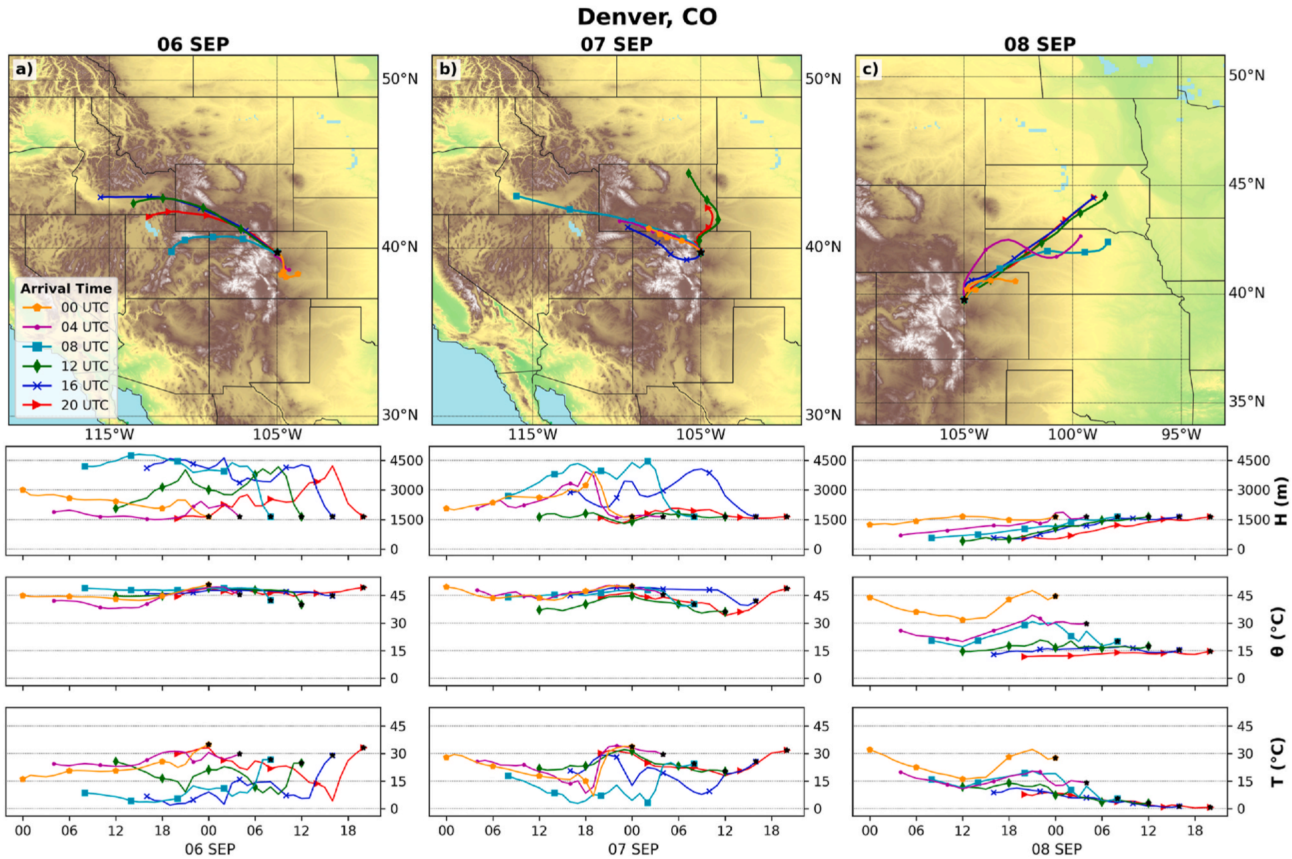

Fig. 12. As in Fig. 7 but for Denver, Colorado.

Acknowledgements

The authors thank Andrew Martin, Katie Straus, and the Ajibade Innovators Team including Ming Ge, Matthew Walter, Jason Sauer, Aswatha Raghunathasami, Jessica Escobar, Arun Pallathadka, Sara Goldstein, Molly Kramer, and Heejun Chang.

References

Abatzoglou, J.T., Kolden, C.A., Williams, A.P., Sadegh, M., Balch, J.K., Hall, A., 2023. Downslope wind-driven fires in the western United States. Earth's Future 11 (5), e2022EF003471. https://doi.org/10.1029/2022EF003471.

Abatzoglou, J.T., Rupp, D.E., O'Neill, L.W., Sadegh, M., 2021. Compound extremes drive the western Oregon wildfires of september 2020. Geophys. Res. Lett. 48 (8), e2021GL092520 https://doi.org/10.1029/2021GL092520.

Blackmon, M.L., Wallace, J.M., Lau, N.-C., Mullen, S.L., 1977. An observational study of the northern hemisphere wintertime circulation. J. Atmos. Sci. 34 (7), 1040–1053. https://doi.org/10.1175/1520-0469(1977)034<1040:AOSOTN>2.0.CO;2.

Branstator, G., 1992. The maintenance of low-frequency atmospheric anomalies. J. Atmos. Sci. 49 (20), 1924–1946. https://doi.org/10.1175/1520-0469(1992)049<1924:TMOLFA>2.0.CO;2.

Braverman, M., Phibbs, S.C., Rau, A., Penner, E., 2021. A Community Health Impact Assessment of the Santiam Canyon: One Year after the 2020 Labor Day Wildfires. Oregon State University. https://health.oregonstate.edu/research/santiam-canyon.

Conrick, R., Mass, C.F., 2023. The influence of soil moisture on the historic 2021 Pacific Northwest heatwave. Mon. Weather Rev. 151 (5), 1213–1228. https://doi.org/10.1175/MWR-D-22-0253.1.

Conrick, R., Mass, C.F., Boomgard-Zagrodnik, J.P., Ovens, D., 2021. The influence of wildfire smoke on cloud microphysics during the september 2020 Pacific Northwest wildfires. Weather Forecast. 36 (4), 1519–1536. https://doi.org/10.1175/WAF-D-21-0044.1.

Garner, J.M., Kovacik, C.E., 2023. Extreme wildfire environments and their impacts occurring with offshore-directed winds across the pacific coast states. Weather, Climate, and Society 15 (1), 75–93. https://doi.org/10.1175/WCAS-D-22-0043.1.

Gedalof, Z., Peterson, D.L., Mantua, N.J., 2005. Atmospheric, climatic, and ecological controls on extreme wildfire years in the northwestern United States. Ecol. Appl. 15 (1), 154–174. https://doi.org/10.1890/03-5116.

Gelaro, R., McCarty, W., Suárez, M.J., Todling, R., Molod, A., Takacs, L., Randles, C.A., Darmenov, A., Bosilovich, M.G., Reichle, R., Wargan, K., Coy, L., Cullather, R., Draper, C., Akella, S., Buchard, V., Conaty, A., Silva, A. M. da, Gu, W., et al., 2017. The Modern-Era Retrospective analysis for Research and Applications, version 2 (MERRA-2). J. Clim. 30 (14), 5419–5454. https://doi.org/10.1175/JCLI-D-16-0758.1.

Hawkins, L.R., Abatzoglou, J.T., Li, S., Rupp, D.E., 2022. Anthropogenic influence on recent severe autumn fire weather in the west coast of the United States. Geophys. Res. Lett. 49 (4), e2021GL095496 https://doi.org/10.1029/2021GL095496.

Hostetler, S.W., Bartlein, P.J., Alder, J.R., 2018. Atmospheric and surface climate associated with 1986–2013 wildfires in North America. J. Geophys. Res.: Biogeosciences 123 (5), 1588–1609. https://doi.org/10.1029/2017JG004195.

Jain, P., Flannigan, M., 2021. The relationship between the polar jet stream and extreme wildfire events in North America. J. Clim. 34 (15), 6247–6265. https://doi.org/10.1175/JCLI-D-20-0863.1.

Juliano, T.W., Jiménez, P.A., Kosović, B., Eidhammer, T., Thompson, G., Berg, L.K., Fast, J., Motley, A., Polidori, A., 2022. Smoke from 2020 United States wildfires responsible for substantial solar energy forecast errors. Environ. Res. Lett. 17 (3), 034010 https://doi.org/10.1088/1748-9326/ac5143.

Loikith, P.C., Kalashnikov, D.A., 2023. Meteorological analysis of the Pacific Northwest june 2021 heatwave. Mon. Weather Rev. 151 (5), 1303–1319. https://doi.org/10.1175/MWR-D-22-0284.1.

Loikith, P.C., Singh, D., Taylor, G.P., 2022. Projected changes in atmospheric ridges over the pacific–North American region using CMIP6 models. J. Clim. 35 (15), 5151–5171. https://doi.org/10.1175/JCLI-D-21-0794.1.

Mass, C.F., Ovens, D., 2019. The northern California wildfires of 8–9 october 2017: the role of a major downslope wind event. Bull. Am. Meteorol. Soc. 100 (2), 235–256. https://doi.org/10.1175/BAMS-D-18-0037.1.

Mass, C.F., Ovens, D., Conrick, R., Saltenberger, J., 2021. The september 2020 wildfires over the Pacific Northwest. Weather Forecast. 36 (5), 1843–1865. https://doi.org/10.1175/WAF-D-21-0028.1.

Millin, O.T., Furtado, J.C., 2022. The role of wave breaking in the development and subseasonal forecasts of the february 2021 Great Plains cold air outbreak. Geophys. Res. Lett. 49 (21), e2022GL100835 https://doi.org/10.1029/2022GL100835.

National Weather Service. September 8-9, 2020 Early Season Snowfall & Record Cold. n. d.-a. https://www.weather.gov/bou/Sept2020EarlySnow.

National Weather Service. September 8-10, 2020 Early Season Winter Storm. n.d.-b. https://www.weather.gov/gjt/08–10September2020_StormSummary.

Nauslar, N.J., Abatzoglou, J.T., Marsh, P.T., 2018. The 2017 north bay and southern California fires: a case study. Fire 1 (1), 1. https://doi.org/10.3390/fire1010018.

Oregon Department of Emergency Management. Wildfires after September 7 2020. n.d. https://experience.arcgis.com/experience/533e2f942b1a49bdb6746a16b68b7981.

Oregon Department of Environmental Quality, 2020. Wildfire Smoke Brings Record Poor Air Quality to Oregon, New Data Shows. https://deqblog.com/2020/09/16/wildfire-smoke-brings-record-poor-air-quality-to-oregon-new-data-shows/.

Oregon Department of Transportation, 2022. 2020 Labor Day Wildfires Hazard Tree and Debris Removal Operations: after Actions Report. https://digital.osl.state.or.us/islandora/object/osl %3A997398.

Pelly, J.L., Hoskins, B.J., 2003. A new perspective on blocking. J. Atmos. Sci. 60 (5), 743–755. https://doi.org/10.1175/1520-0469(2003)060<0743:ANPOB>2.0.CO;2.

Rasmussen, M., Lord, R., Fay, R., Baribault, T., Goodnow, R., 2021. 2020 Labor Day Fires: Economic Impacts to Oregon's Forest Sector. Oregon Forest Resources Institute. https://oregonforests.org/pub/2020-labor-day-fires-economic-impacts.

Reilly, M.J., Zuspan, A., Halofsky, J.S., Raymond, C., McEvoy, A., Dye, A.W., Donato, D. C., Kim, J.B., Potter, B.E., Walker, N., Davis, R.J., Dunn, C.J., Bell, D.M., Gregory, M. J., Johnston, J.D., Harvey, B.J., Halofsky, J.E., Kerns, B.K., 2022. Cascadia Burning: the historic, but not historically unprecedented, 2020 wildfires in the Pacific Northwest, USA. Ecosphere 13 (6), e4070. https://doi.org/10.1002/ecs2.4070.

Rolph, G., Stein, A., Stunder, B., 2017. Real-time environmental Applications and Display sYstem: READY. Environ. Model. Software 95, 210–228. https://doi.org/10.1016/j.envsoft.2017.06.025.

Sharma, A.R., Jain, P., Abatzoglou, J.T., Flannigan, M., 2022. Persistent positive anomalies in geopotential heights promote wildfires in Western NorthNorth America. J. Clim. 35 (19), 6469–6486. https://doi.org/10.1175/JCLI-D-21-0926.1.

Stein, A.F., Draxler, R.R., Rolph, G.D., Stunder, B.J.B., Cohen, M.D., Ngan, F., 2015. NOAA's HYSPLIT atmospheric transport and dispersion modeling system. Bull. Am. Meteorol. Soc. 96 (12), 2059–2077. https://doi.org/10.1175/BAMS-D-14-00110.1.

Stuivenvolt-Allen, J., Simon Wang, S.-Y., LaPlante, M.D., Yoon, J.-H., 2021. Three western pacific typhoons strengthened fire weather in the recent northwest U.S. Conflagration. Geophys. Res. Lett. 48 (3), e2020GL091430 https://doi.org/10.1029/2020GL091430.

Trenga, C.A., 2023. Air Quality and Asthma-like Illness in Oregon during Wildfires. Centers for Disease Control and Prevention. https://www.cdc.gov/nssp/success-stories/Air-Quality-and-Asthma-like-Illness-in-Oregon-During-Wildfires.html.

Trouet, V., Taylor, A.H., Carleton, A.M., Skinner, C.N., 2009. Interannual variations in fire weather, fire extent, and synoptic-scale circulation patterns in northern California and Oregon. Theor. Appl. Climatol. 95 (3), 349–360. https://doi.org/10.1007/s00704-008-0012-x.

US Centers for Disease Control and Prevention, 2023. Wildfire Smoke and COVID-19. Natural Disasters and Severe Weather. https://www.cdc.gov/disasters/covid-19/wildfire_smoke_covid-19.html.

US Environmental Protection Agency, n.d. Air Quality System Data Mart [Internet database]. Retrieved March 13, 2023, from https://www.epa.gov/outdoor-air-quality-data.

Vose, R.S., Easterling, D.R., Kunkel, K.E., LeGrande, A.N., Wehner, M.F., 2017. Temperature changes in the United States. In: Wuebbles, D.J., Fahey, D.W., Hibbard, K.A., Dokken, D.J., Stewart, B.C., Maycock, T.K. (Eds.), Climate Science Special Report: Fourth National Climate Assessment, vol. I. U.S. Global Change Research Program, Washington, DC, USA, pp. 185–206. https://doi.org/10.7930/J0N29V45.

Zhong, S., Yu, L., Heilman, W.E., Bian, X., Fromm, H., 2020. Synoptic weather patterns for large wildfires in the northwestern United States—a climatological analysis using three classification methods. Theor. Appl. Climatol. 141 (3), 1057–1073. https://doi.org/10.1007/s00704-020-03235-y.

Zhou, X., Josey, K., Kamareddine, L., Caine, M.C., Liu, T., Mickley, L.J., Cooper, M., Dominici, F., 2021. Excess of COVID-19 cases and deaths due to fine particulate matter exposure during the 2020 wildfires in the United States. Sci. Adv. 7 (33), eabi8789 https://doi.org/10.1126/sciadv.abi8789.